J|A|C|S ARTICLES

Published on Web 06/28/2010

Probing Valence Orbital Composition with Iron Kβ X-ray Emission Spectroscopy

Nicole Lee,[†] Taras Petrenko,[‡] Uwe Bergmann,*[,§] Frank Neese,*[,‡] and Serena DeBeer*[,†]

Department of Chemistry and Chemical Biology, Cornell University, Ithaca, New York 14853, Institut für Physikalische und Theoretische Chemie, Universität Bonn, D-53115 Bonn, Germany, and Linac Coherent Light Source, SLAC National Accelerator Laboratory, Menlo Park, California 94025

Received February 12, 2010; E-mail: bergmann@slac.stanford.edu; neese@thch.uni-bonn.de; sdg63@cornell.edu

Abstract: A systematic study of 12 ferric and ferrous Kβ X-ray emission spectra (XES) is presented. The factors contributing to the Kβ main line and the valence to core region of the spectra are experimentally assessed and quantitatively evaluated. While the Kβ main line spectra are dominated by spin state contributions, the valence to core region is shown to have greater sensitivity to changes in the chemical environment. A density functional theory (DFT) based approach is used to calculate the experimental valence spectra and to evaluate the contributions to experimental intensities and energies. The spectra are found to be dominated by iron np to 1s electric dipole allowed transitions, with pronounced sensitivity to spin state, ligand identity, ligand ionization state, hybridization state, and metal−ligand bond lengths. These findings serve as an important calibration for future applications to iron active sites in biological and chemical catalysis. Potential applications to Compound II heme derivatives are highlighted.

Introduction

Iron-containing active sites form the catalytic cores of numerous metalloenzymes, which are responsible for the activation of small molecules. These include nitrogenase[1,2] (which converts dinitrogen to ammonia) as well as cytochrome P450[3,4] and methane monooxygenase[5] (both which enable alkane hydroxylation). The ability of metalloenzymes to carry out remarkably difficult chemical transformations has inspired decades of research aimed at understanding the correlations between structure and function. Ultimately, this requires a clear description of the ground state geometric and electronic structure, as well as the structures of the intermediates in the reaction cycles. It is here that spectroscopic methods have played a key role. Electron paramagnetic resonance (EPR) and Mössbauer studies have provided details on the spin state and oxidation state of numerous iron active sites, including reaction intermediates.[6,7] Complementary information has been obtained utilizing X-ray absorption spectroscopy (XAS), where the shift in the Fe K-edge energy provides a measure of effective nuclear charge on the absorbing atom, and the intensity of pre-edge transitions provides information on the local site symmetry.[8,9] In addition, extended X-ray absorption fine structure (EXAFS) is frequently utilized to obtain parameters for the coordination number, type, and distance of ligating atoms with respect to the absorber.[10] Yet, often, key questions remain, and many are focused on the identity of coordinated ligands. These include fundamental questions such as the nature of the central atom (C, N, or O) in nitrogenase,[11,12] the nature of the oxygen binding mode in methane monooxygenase,[13] and the protonation state of ferryl intermediates.[14,15] These challenges arise in part due to inherent limitations of the currently employed experimental methods. For instance, EXAFS cannot distinguish between similar scatterers (i.e., C, N, O), and protonation states of the scatterers can only be indirectly inferred based on bond lengths. As EXAFS has intrinsic limitations in its resolution, in many cases the individual metal−ligand bonds cannot be uniquely

[†] Cornell University.
[‡] Universität Bonn.
[§] SLAC National Accelerator Laboratory.

(1) Burgess, B. K.; Lowe, D. L. *Chem. Rev.* **1996**, *96*, 2983.
(2) Hoffman, B. M.; Dean, D. R.; Seefeldt, L. C. *Acc. Chem. Res.* **2009**, *42*, 609.
(3) Denisov, I. G.; Makris, T. M.; Sligar, S. G.; Schlichting, I. *Chem. Rev.* **2005**, *105*, 2253.
(4) Sono, M.; Roach, M. P.; Coulter, E. D.; Dawson, J. H. *Chem. Rev.* **1996**, *96*, 2841.
(5) Wallar, B. J.; Lipscomb, J. D. *Chem. Rev.* **1996**, *96*, 2625.
(6) Krebs, C.; Fujimori, D. G.; Walsh, C. T.; Bollinger, J. M., Jr. *Acc. Chem. Res.* **2007**, *40*, 484.
(7) Solomon, E. I.; Brunold, T. C.; Davis, M. I.; Kemsley, J. N.; Lee, S. K.; Lehnert, N.; Neese, F.; Skulan, A. J.; Yang, Y. S.; Zhou, J. *Chem. Rev.* **2000**, *100*, 235.
(8) Roe, A. L.; Schneider, D. J.; Mayer, R. J.; Pyrz, W.; Widom, J.; Que, L., Jr. *J. Am. Chem. Soc.* **1984**, *106*, 1676.
(9) Westre, T. E.; Kennepohl, P.; DeWitt, J. G.; Hedman, B.; Hodgson, K. O.; Solomon, E. I. *J. Am. Chem. Soc.* **1997**, *119*, 6297.
(10) Levina, A.; Armstrong, R. S.; Lay, P. A. *Coord. Chem. Rev.* **2005**, *249*, 141.
(11) Einsle, O.; Tezcan, F. A.; Andrade, S. L. A.; Schmid, B.; Yoshida, M.; Howard, J. B.; Rees, D. C. *Science* **2002**, *297*, 1696.
(12) Howard, J. B.; Rees, D. C. *Proc. Natl. Acad. Sci. U.S.A.* **2006**, *103*, 17088.
(13) Xue, G. Q.; Fiedler, A. T.; Martinho, M.; Munck, E.; Que, L. *Proc. Natl. Acad. Sci. U.S.A.* **2008**, *105*, 20615.
(14) Green, M. T.; Dawson, J. H.; Gray, H. B. *Science* **2004**, *304*, 1653.
(15) Newcomb, M.; Halgrimson, J. A.; Horner, J. H.; Wasinger, E. C.; Chen, L. X.; Sligar, S. G. *Proc. Natl. Acad. Sci. U.S.A.* **2008**, *105*, 8179.

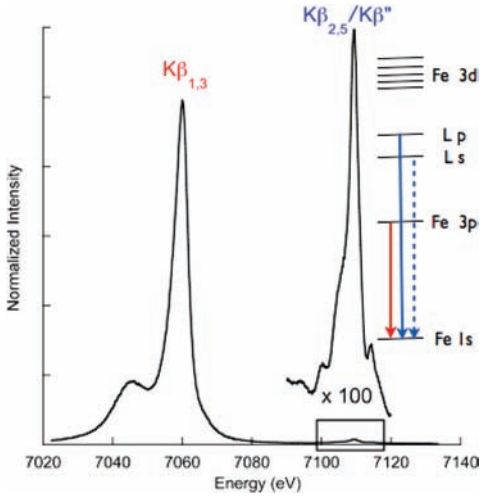

Figure 1. Fe Kβ XES spectrum for $[Fe(III)Cl_4]^{1-}$. The box indicates the valence to core region of the spectrum, which has been expanded by 100-fold above. A simplified energy diagram showing the origin of the K$\beta_{1,3}$ and valence to core transitions is given on the right.

determined. While isotope substitution provides a means to distinguish C, N, and O atoms by EPR or vibrational methods, such experiments pose a challenge in a protein matrix, due in part to the abundance of these elements and difficulties endemic to isotopic substitution.

These challenges, however, may be addressed by Fe Kβ X-ray emission spectroscopy (XES).[16] Though Kβ XES phenomena have been known for some time,[17] recent developments of high-resolution spectrometers in the hard X-ray range, utilizing synchrotron sources, have provided greater accessibility to these types of measurements. However, very few Kβ XES studies have been performed on structurally well-characterized, low molecular weight model complexes, and as such, many questions remain about the factors governing the intensities, energies, and relative distributions of spectral features.[18,19] Here we focus on the development of Fe Kβ XES as a quantitative probe of iron active site structure, including metal spin state,[20,21] oxidation state, and ligand identity. Kβ XES involves following the emission of photons by decay of electrons after ionization of the metal 1s electron (Figure 1). The K$\beta_{1,3}$ emission line corresponds to an electric dipole allowed 3p−1s transition, which will have significant contributions from 3p−3d electron exchange interactions as well as 3p spin−orbit coupling (SOC) contributions.[16] To higher energy are transitions that correspond to valence electron transitions into the metal 1s core hole, the so-called K$\beta_{2,5}$/Kβ (or valence to core) region. These transitions have been previously assigned as ligand np to metal 1s (K$\beta_{2,5}$) and ligand ns to metal 1s ("Kβ" or "satellite") transitions.[22,23] However, the selection rules governing the intensities and the contribution of oxidation state, spin state, and ligand identity have not been investigated in detail.

Here, we present a systematic study of the Kβ XES spectra of 12 ferrous and ferric complexes in high- and low-spin states. The oxidation and spin state dependent changes of both the Kβ main line and the valence to core region are identified. Though the spin state dependence of the Kβ main line has been previously investigated,[24,25] to our knowledge the spin state contribution to the valence to core region has not been previously noted. In addition, the contributions of site symmetry, oxidation state, and ligand identity to the iron valence to core spectra are investigated and quantitatively assessed.

The experimental valence to core spectra are correlated to calculated spectra, which have been obtained using a straightforward density functional theory (DFT) approach. The strong correlation between experiment and theory not only validates the computational protocol but also indicates that these spectra can be used as a quantitative map of valence orbital composition. This also allows us to individually assess the contributions of symmetry, spin state, metal−ligand bond lengths, and ligand identity in an in silico fashion The potential of these methods for identifying subtle perturbations in biological iron active site structures is discussed and illustrated by pilot calculations on the compound II intermediate in cytochrome P450.

Experimental Procedures

Sample Preparation. $K_3[Fe(CN)_6]$, $K_4[Fe(CN)_6]$, and $[Fe(bipy)_3](PF6)_2$ (where bipy = 2,2′-bipyriine) were purchased from Aldrich and used without further purification. [Fe(tpfp)Cl] (where tpfp = tetra(pentafluoro)phenylporphyrin) was purchased from Frontier Scientific. $[Et_4N]_2[FeCl_4]$,[26] $(Et_4N)[FeCl_4]$,[27] NaK_3FeCl_6,[28] $[Fe(acac)_3]$,[29] $[Fe(tacn)_2]Cl_3$,[30] $[Fe(tacn)_2]Cl_2$,[30] [Fe(III)(tpp)(ImH)$_2$]Cl,[31] and $[Fe(II)(MeIm)_6][B(C_6H_5)_4]_2$[32] were prepared according to published procedures (acac = acetylacetonate, tacn = 1,4,7-tiazacyclononane, tpp = tetraphenylporphyrin, MeIm = *N*-methyl-imidazole). All samples were prepared as dilutions in boron nitride, pressed into 1 mm Al spacers, and sealed with 38 μm Kapton tape. All ferrous samples were prepared in an inert atmosphere glovebox. A complete list of all samples, including the oxidation state, spin state, and iron site symmetry, is given in Table 1.

XES Measurements. All XES data were collected at SSRL beamline 6-2 (54-pole wiggler, 1 T). The incident energy was set to 9 keV utilizing at Si(111) a liquid nitrogen cooled monochromator. Vertical and horizontal focusing mirrors were used to achieve a beam size of 200 × 800 μm with a flux of ~4×10^{12} photons/s at 100 mA. The energy of the incident beam was calibrated with an iron foil, setting the first inflection point to 7111.2 eV.

(16) Glatzel, P.; Bergmann, U. *Coord. Chem. Rev.* **2005**, *249*, 65.
(17) (a) Kasrai, M.; Urch, D. S. *J. Chem. Soc., Faraday Trans. 2* **1979**, *75*, 1522. (b) Tsutsumi, K. *J. Phys. Soc. Jpn.* **1959**, *14*, 1696.
(18) Smolentsev, G.; Soldatov, A. V.; Messinger, J.; Merz, K.; Weyhermuller, T.; Bergmann, U.; Pushkar, Y.; Yano, J.; Yachandra, V. K.; Glatzel, P. *J. Am. Chem. Soc.* **2009**, *131*, 13161.
(19) Pushkar, Y.; Long, X.; Glatzel, P.; Brudvig, G. W.; Dismukes, G. C.; Collins, T. J.; Yachandra, V. K.; Yano, J.; Bergmann, U. *Angew. Chem., Int. Ed.* **2009**, *48*, 800.
(20) (a) Vanko, G.; de Groot, F. M. F. *Phys. Rev. B* **2007**, *75*, 177101. (b) Vanko, G.; Neisius, T.; Molnar, G.; Renz, F.; Karpati, S.; Shukla, A.; de Groot, F. M. F. *J. Phys. Chem. B* **2006**, *110*, 11647. (c) Antonov, V. N.; Germash, L. P.; Shpak, A. P.; Yaresko, A. N. *Phys. Status Solidi B* **2009**, *246*, 411.
(21) Lengsdorf, R.; Rueff, J. P.; Vanko, G.; Lorenz, T.; Tjeng, L. H.; Abd-Elmeguid, M. M. *Phys. Rev. B* **2007**, *75*, 180401.
(22) Bergmann, U.; Horne, C. R.; Collins, T. J.; Workman, J. M.; Cramer, S. P. *Chem. Phys. Lett.* **1999**, *302*, 119.
(23) Bergmann, U.; Bendix, J.; Glatzel, P.; Gray, H. B.; Cramer, S. P. *J. Chem. Phys.* **2002**, *116*, 2011.
(24) Glatzel, P.; Bergmann, U.; de Groot, F. M. F.; Cramer, S. P. *Phys. Rev. B* **2001**, *64*, 045109.
(25) Peng, G.; Degroot, F. M. F.; Hamalainen, K.; Moore, J. A.; Wang, X.; Grush, M. M.; Hastings, J. B.; Siddons, D. P.; Armstrong, W. H.; Mullins, O. C.; Cramer, S. P. *J. Am. Chem. Soc.* **1994**, *116*, 2914.
(26) Lauher, J. W.; Ibers, J. A. *Inorg. Chem.* **1975**, *14*, 348.
(27) Kistenmacher, T. J.; Stucky, G. D. *Inorg. Chem.* **1968**, *7*, 2150.
(28) Beattie, J. K.; Moore, C. J. *Inorg. Chem.* **1982**, *21*, 1292.
(29) Iball, J.; Morgan, C. H. *Acta Crystallogr.* **1967**, *23*, 239.
(30) Wieghardt, K.; Schmidt, W.; Herrmann, W.; Kuppers, H. J. *Inorg. Chem.* **1983**, *22*, 2953.
(31) Scheidt, W. R.; Osvath, S. R.; Lee, Y. J. *J. Am. Chem. Soc.* **1987**, *109*, 1958.
(32) Miller, L. L.; Jacobson, R. A.; Chen, Y. S.; Kurtz, D. M. *Acta Crystallogr. C* **1989**, *45*, 527.

Table 1. Oxidation States, Spin States, Geometries, and Crystallographic Structure References for the Iron Model Complexes Investigated by XES

complex	Fe oxidation state	spin state	geometry	crystal structure reference
$[FeCl_4]^{1-}$	III	5/2	T_d	27
$[Fe(acac)_3]^0$	III	5/2	O_h	29
$[Fe(tpfp)Cl]^0$	III	5/2	C_{4v}	33
$[Fe(CN)_6]^{3-}$	III	1/2	O_h	34
$[Fe(tacn)_2]^{3+}$	III	1/2	O_h	30
$[Fe(tpp)(ImH)_2]^{1+}$	III	1/2	D_{4h}	31
$[FeCl_4]^{2-}$	II	2	T_d	26
$[FeCl_6]^{4-}$	II	2	O_h	28
$[Fe(bipy)_3]^{2+}$	II	2	O_h	35
$[Fe(MeIm)_6]^{2+}$	II	2	O_h	32
$[Fe(CN)_6]^{4-}$	II	0	O_h	36
$[Fe(tacn)_2]^{2+}$	II	0	O_h	37

XES spectra were recorded with a crystal array spectrometer, which employs three spherically bent Ge(620) crystals (100 mm diameter, 1 m radius of curvature) aligned on intersecting Rowland circles (the schematic setup is shown, e.g., in Figure 5 in ref 16). An energy resolving Si drift detector (Vortex or Ketek) with a 3 mm vertical slit was used as the X-ray photon detector. Samples were positioned at 45 degrees with respect to the incident beam and were maintained at a temperature of 10 K in an Oxford CF1208 continuous flow liquid helium cryostat. A helium-filled flight path was utilized between the cryostat and the spectrometer to minimize signal attenuation of the fluorescence.

Iron Kβ XES spectra were collected from 7020 to 7120 eV, with a step size of ∼0.2 eV over the $K\beta_{1,3}$ main line (7020−7070 eV) and steps of ∼0.15 eV over the valence to core region (7070−7120 eV). Spectra were normalized to the incident flux I_0 measured in a He-filled ion chamber. The spectrometer energy was calibrated by measuring the energy of the elastically scattered beam as a function of spectrometer position using a monochromator calibration of 7111.2 eV for the first derivative maximum of the Fe metal XANES. The spectrometer energy resolution is estimated at ∼1.4 eV full width at half-maximum (fwhm) by Gaussian deconvolution of the measured elastic peak widths (1.6−1.8 eV fwhm) using the theoretical Darwin width of ∼1.0 eV fwhm for the Si(111) monochromator. This compares to a Lorentzian core hole lifetime broadening of ∼1.5 eV for Fe Kβ XES spectra (given by the sum of the metal 1s broadening (1.3 eV) and the metal 3p, np, or ligand 2s broadenings, respectively). However, emission spectra are further broadened by mutiplet effects. Fe_2O_3 was used as a reference sample for calibrating the spectrometer energy between different experimental runs, with the maximum of the $K\beta_{1,3}$ main line calibrated to 7060.6 eV and the maximum of the $K\beta_{2,5}$ line calibrated to 7107.2 eV.

For all samples, radiation damage studies were performed, and the maximum exposure time per spot was determined. Multiple spots were utilized on each sample, and the averaged data represent only those scans which showed no evidence of radiation damage. The total integrated area of the averaged spectra was set to a value of 1. The valence to core region was fit using the program EDG_FIT.[38] The background tail from the $K\beta_{1,3}$ main line and the valence to core features were modeled using pseudo-Voigt line shapes (simple sums of Gaussian and Lorenztian functions). The tail from the $K\beta_{1,3}$ background was subtracted from the reported areas in Table 2. Representative fits to the data are given in the Supporting Information. Reported areas are the average of all good fits (with an estimated error of ∼10%). All areas have been multiplied by 1000.

Table 2. Energies and Areas for Fe Kβ XES Spectra

complex	$K\beta_{1,3}$ energy (eV)	$K\beta_{2,5}$ energy (eV)	area (valence to core region)[a]
High-Spin Fe(III)			
$[FeCl_4]^{1-}$	7060.4	7109.8	10.3
$[Fe(acac)_3]^0$	7060.0	7104.2	12.3
$[Fe(tpfp)Cl]^0$	7060.1	7108.8	8.5
Low-Spin Fe(III)			
$[Fe(CN)_6]^{3-}$	7057.8	7106.1	21.7
$[Fe(tacn)_2]^{3+}$	7059.1	7109.3	16.3
$[Fe(tpp)(ImH)_2]^{1+}$	7058.8	7108.3	16.3
High-Spin Fe(II)			
$[FeCl_4]^{2-}$	7059.6	7108.7	9.3
$[FeCl_6]^{4-}$	7060.3	7108.8	6.9
$[Fe(bipy)_3]^{2+}$	7060.1	7107.3	11.4
$[Fe(MeIm)_6]^{2+}$	7060.3	7108.8	8.8
Low-Spin Fe(II)			
$[Fe(CN)_6]^{4-}$	7056.8	7104.8	24.5
$[Fe(tacn)_2]^{2+}$	7058.5	7107.8	17.0

[a] The reported areas are based on fits to the normalized data and have been multiplied by 1000. The reported areas are the average of all good fits (estimated errors are ∼10%).

XES Calculations. All calculations were performed with the ORCA quantum chemistry program[39] using the theoretical protocol summarized in the text. The Fe valence to core XES spectra of all complexes were calculated using both the experimental X-ray structures (method 1, as referenced in Table 1) and geometry optimized structures (method 2). Geometry optimizations were performed using the BP86 functional, the zeroth-order regular approximation for relativistic effects (ZORA)[40] following the model potential implementation of van Wüllen,[41] and the scalar-relativistically recontracted def2-TZVP(-f) basis set.[42] The negative charge on the complexes was compensated with the conductor-like screening model (COSMO) in an infinite dielectric. Molecular orbitals were visualized using Chimera.[43]

For all XES calculations presented in this study, the BP86 functional[44,45] was utilized in conjunction with the CP(PPP) basis set[46] for the Fe (with a special integration accuracy of 7) and the TZVP basis set for all other atoms. Calculations were carried out in a dielectric continuum using the conductor-like screening model (COSMO)[47] in an infinite dielectric. The calculations used a dense integration grid (ORCA Grid4). This combination of basis set and functional has previously proven successful for TDDFT calculation

(33) Song, B.; Swenson, D. C.; Goff, H. M. *Acta Crystallogr., Sect. C* **1998**, *54*, IUC9800058.
(34) Overgaard, J.; Svendsen, H.; Chevalier, M. A.; Iversen, B. B. *Acta Crystallogr.* **2005**, *E61*, m268.
(35) Figgis, B. N.; Skelton, B. W.; White, A. H. *Aust. J. Chem.* **1978**, *31*, 57.
(36) Kuchár, J.; Cernák, J.; Massa, W. *Acta Crystallogr.* **2004**, *C60*, m418.
(37) Boeyens, J. C. A.; Forbes, A. G. S.; Hancock, R. D.; Wieghardt, K. *Inorg. Chem.* **1985**, *24*, 2926.
(38) George, G. N. *EXAFSPAK, SSRL, SLAC*; Stanford University: Stanford, CA, 2000.
(39) Neese, F.; Becker, U.; Ganyushin, D.; Hansen, A.; Liakos, D. G.; Kollmar, C.; Kossmann, S.; Petrenko, T.; Reimann, C.; Riplinger, C.; Sivalingam, K.; Valeev, E.; Wezisla, B.; Wennmohs, F. *ORCA: An ab initio, DFT, and Semiempirical Electronic Structure Package*, version 2.7.0; University of Bonn: Bonn, Germany, 2009.
(40) van Lenthe, E.; van der Avoird, A.; Wormer, P. E. S. *J. Chem. Phys.* **1998**, *108*, 478.
(41) van Wüllen, C. *J. Chem. Phys.* **1998**, *109*, 392.
(42) Pantazis, D. A.; Chen, X. Y.; Landis, C. R.; Neese, F. *J. Chem. Theory Comput.* **2008**, *4*, 908.
(43) Pettersen, E. F.; Goddard, T. D.; Huang, C. C.; Couch, G. S.; Greenblatt, D. M.; Meng, E. C.; Ferrin, T. E. *J. Comput. Chem.* **2004**, *13*, 1605.
(44) Becke, A. D. *Phys. Rev. A* **1988**, *38*, 3098.
(45) Perdew, J. P. *Phys. Rev. B* **1986**, *33*, 8822.
(46) Neese, F. *Inorg. Chim. Acta* **2002**, *337C*, 181.
(47) Klamt, A.; Schüürmann, G. *J. Chem. Soc., Perkin. Trans.* **1993**, *2*, 799.

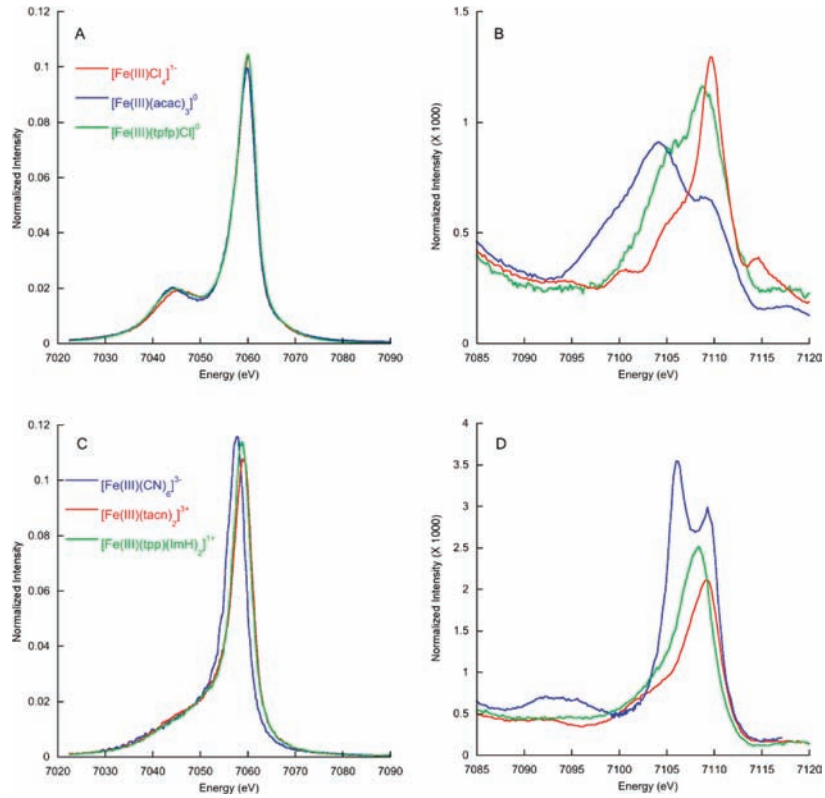

Figure 2. Fe Kβ main line XES spectra for high-spin ferric complexes (A). Valence to core region for the complexes shown in A (B). Fe Kβ main line XES spectra for low-spin ferric complexes (C). Valence to core region for the complexes shown in C (D).

of XAS spectra.[48−50] A detailed investigation of the contribution of the functional, basis sets, and scalar relativistic effects to the calculated XES spectra will be the focus of a future study.

Results and Analysis

Kβ XES Spectra: Ferric Complexes. The normalized Fe Kβ XES spectra for the high-spin ferric complexes $[FeCl_4]^{1-}$, $[Fe(acac)_3]^0$, and $[Fe(tpfp)Cl]^0$ are shown in Figure 2, with the Kβ main line spectra given in 2A and an expansion of the corresponding valence to core region given in 2B. All of the high-spin ferric complexes are characterized by a K$\beta_{1,3}$ main line with a maximum at ∼7060 eV (Table 2) and a Kβ' feature at ∼7045 eV. The Kβ' feature arises from mutiplet effects and can be modeled through inclusion of electron−electron interactions; however, this is not the focus of the present study.[24,25] The valence to core region of the spectra is characterized by a broad envelope of transitions (between 7100 and 7115 eV) with maxima at ∼7105−7109 eV and integrated areas of 8−12 units of intensity (Table 2). While the Kβ main line spectra are essentially identical to each other, the valence to core spectra show clear variations in the energy and intensity distributions, indicating that these spectra are much more sensitive to a change in ligation than the Kβ main line.

Figures 2C and D show the Kβ main line spectra and valence to core spectra, respectively, for a series of low-spin ferric complexes $([Fe(III)(CN)_6]^{3-}$, $[Fe(III)(tacn)_2]^{3+}$, and $[Fe(III)(tpp)(ImH)_2]^{1+})$. In contrast to the high-spin complexes, the Kβ main line spectra no longer have a distinct Kβ' feature, and the peak maximum has decreased in energy by ∼1−2 eV, consistent with a decrease in spin state.[16] There are also pronounced changes in the valence to core region of the spectra. In this spectral region, the transition envelope is generally narrower (7102−7113 eV) for the low-spin complexes, and the integrated area relative to the full spectral range has increased by a factor of 2 or more (16−22 units, Table 2) over that of the high-spin complexes. Again, the valence to core region shows a much greater variation in energy and intensity distribution as compared to the Kβ main line, demonstrating the strongly increased sensitivity to the ligand environment.

Kβ XES Spectra: Ferrous Complexes. The normalized Fe Kβ XES spectra for a series of high-spin and low-spin ferrous complexes are given in Figure 3A,B and 3C,D, respectively. Similar to the high-spin ferric complexes, the high-spin ferrous complexes $([FeCl_4]^{2-}$, $[FeCl_6]^{4-}$, $[Fe(bipy)_3]^{2+}$, and $[Fe(MeIm)_6]^{2+})$ all exhibit a pronounced Kβ' feature at ∼7045 eV in the Kβ main line spectra, with a maximum at ∼7060 eV (Figure 3A). Comparison of $[Fe(III)Cl_4]^{1-}$ to $[Fe(II)Cl_4]^{2-}$ shows a 0.8 eV decrease in energy upon reduction, which may be attributed to the decrease in spin state from $S = 5/2$ to $S = 2$. However, care must be taken in using the energy of the Kβ main line as an isolated indicator of spin state as there is clear overlap in the $S = 2$ and $S = 5/2$ Kβ energies (Table 2). The valence to core region of the high-spin ferrous spectra shows greater spectral variation and has integrated areas of 7−11 units of intensity, very similar to what is observed for the high-spin ferric complexes. Interestingly, the maximum peak energy in the valence to core region decreases by 1.2 eV going from $[Fe(III)Cl_4]^{1-}$ to $[Fe(II)Cl_4]^{2-}$. This indicates that there are different contributions to the observed energy shift in the K$\beta_{1,3}$ vs valence to core region of the spectra. While the Kβ main

(48) DeBeer George, S.; Petrenko, T.; Neese, F. *J. Phys. Chem. A* **2008**, *112*, 12936.
(49) DeBeer George, S.; Petrenko, T.; Neese, F. *Inorg. Chim. Acta* **2008**, *361*, 965.
(50) DeBeer George, S.; Neese, F. *Inorg. Chem.* **2010**, *49*, 1849.

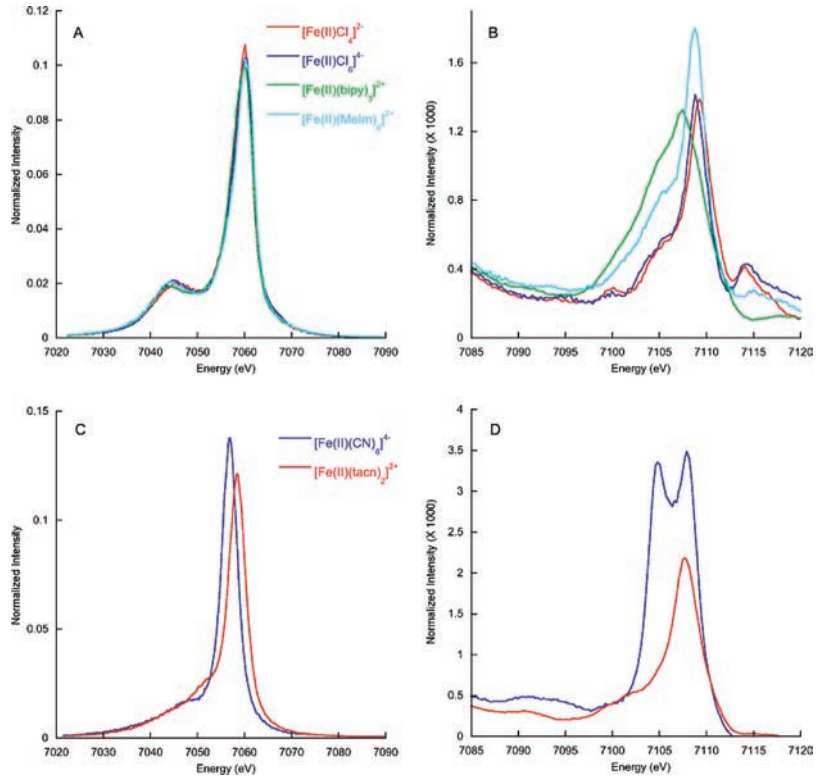

Figure 3. Fe Kβ main line XES spectra for high-spin ferrous complexes (A). Valence to core region for the complexes shown in A (B). Fe Kβ main line XES spectra for low-spin ferrous complexes (C). Valence to core region for the complexes shown in C (D).

line energies are most likely dominated by 3p−3d exchange interactions,[16] the valence to core region likely has a larger contribution due to a change in the effective nuclear charge (Z_{eff}) on the metal.

It is also of interest to note that the K$\beta_{1,3}$ main line and valence to core spectra of T_d-$[FeCl_4]^{2-}$ and O_h-$[FeCl_6]^{4-}$ are essentially identical. This indicates that the iron site symmetry is not a significant factor in determining the spectral intensity. As will be further developed below, this result also provides experimental evidence that these transitions are dominantly dipole allowed in origin and is consistent with previous Mn Kβ XES studies by Glatzel et al.[18]

Ongoing to the low-spin ferrous complexes, the K$\beta_{1,3}$ spectra (analogous to the low-spin ferric complexes) show no Kβ' feature at 7045 eV. However, there is evidence for a weaker shoulder at ∼7050 eV, indicating that upon decreasing spin state the shoulder and the main peak move closer in energy. The K$\beta_{1,3}$ peak maximum is shifted down in energy by several electronvolts relative to the high-spin ferrous complexes, again reflecting a decrease in 3p−3d exchange correlation due to a decrease in spin. Examination of the valence to core region shows that the low spin ferrous complexes have 2−3 times greater intensity than the high-spin complexes, paralleling the trend observed for the ferric complexes. Comparing the ferrous complexes to the analogous ferric complexes, a smaller decrease in the K$\beta_{1,3}$ peak maximum (0.6−1 eV) is observed upon reduction relative to the shift in the valence to core region (1.3−1.5 eV). These data suggest the valence to core region is thus a more sensitive probe of the changes in effective nuclear charge.

From these data, several general trends emerge. The Kβ main line is most sensitive to the spin state on the Fe, with the overall Kβ line shape providing a clear indicator for high-spin complexes (due to the presence of a 7045 eV shoulder) or low-spin complexes. This is consistent with previous XES studies on, e.g., Mn (see ref 16 and references therein). This region of the spectrum is essentially insensitive to the ligand environment. In contrast, the valence to core region shows sensitivity to oxidation state, spin state, *and* changes in the ligand environment. Changes in oxidation state result in ∼1−1.5 eV decreases in energy upon reduction, while differences in spin state are correlated with an increase in valence to core intensity upon decreasing spin state. A change in the coordination environment results in alteration of the overall spectral shape and intensity distribution. This will be systematically investigated below through electronic structure calculations.

Calculation of Valence to Core XES Spectra. To better understand the experimental trends and their origins, we have utilized density functional theory calculations to predict the valence to core region of the XES spectra.

Theory. The total number of photons emitted per unit time I_{IF} that correspond to the transition of an initial core-ionized or core-excited state $|I\rangle$ to the final state $|F\rangle$ in the limit of low concentration of the absorbing species and small path length of the incident beam is given by

$$I_{IF} = W_{GI}\Delta N\frac{A_{IF}}{D_I} \tag{1}$$

where ΔN is the total number of absorbing species in the irradiated volume, and W_{GI} is the transition rate between the ground state $|G\rangle$ and state $|I\rangle$ (capital letters are used for many electron states, lowercase letters for orbitals). W_{GI} is related to the photoionization cross section $\sigma_{GI}(\omega_0)$ at the incident photon frequency ω_0 as

$$W_{GI} = \sigma_{GI}(\omega_0) I_0 \tag{2}$$

The emission rate corresponding to the transition of state $|I\rangle$ to state $|F\rangle$ is given by the Einstein coefficient A_{IF} which is proportional to the emission oscillator strength f_{IF}[51]

$$A_{IF} = -3 f_{IF} \gamma_{\mathrm{el}} \tag{3}$$

where γ_{el} is the classical radiative decay rate of the single-electron oscillator at frequency ω_{IF} which is equal to the transition frequency between the initial and final states (CGS units)

$$\gamma_{\mathrm{el}} = \frac{2e^2\omega_{IF}^2}{3m_e c^3} \tag{4}$$

Here, m_e is the mass of the electron; e is the electron charge; c is the speed of light; and D_I is the total decay rate of the core-excited state $|I\rangle$ which is the sum of the radiative (D_I^{R}) and nonradiative (D_I^{N}) decay rates

$$\begin{aligned} D_I &= D_I^{\mathrm{R}} + D_I^{\mathrm{N}} \\ D_I^{\mathrm{R}} &= \sum_{F'} A_{IF'} \end{aligned} \tag{5}$$

According to eqs 1−4, the relative intensities of different transitions in the XES spectrum can be written as

$$I_{IF}^{\mathrm{R}} = \frac{\omega_{IF}^2 f_{IF}}{\sum_{F'} \omega_{IF'}^2 f_{IF'}} \tag{6}$$

Then, the normalized XES spectrum $I_I^{\mathrm{R}}(\omega_{\mathrm{em}})$ corresponding to emission from state $|I\rangle$ is

$$I_I^{\mathrm{R}}(\omega_{\mathrm{em}}) = \sum_F I_{IF}^{\mathrm{R}} L(\omega_{\mathrm{em}}, \omega_{IF}, \Gamma, \sigma) \tag{7}$$

where $L(\omega_{\mathrm{em}}, \omega_{\mathrm{IF}}, \Gamma, \sigma)$ is a line shape function which, in general, depends on homogeneous (Γ) and inhomogeneous (σ) broadening parameters. From eq 7 it follows that the calculated XES spectrum has an integrated area of unity ($\int I^{\mathrm{R}}(\omega_{\mathrm{em}}) = 1$) and thus can be directly compared with the normalized experimental XES spectrum. In this work, we take the line shape function to be a Gaussian function, but other choices such as a Voigt shape may be more appropriate if a mixture of homogeneous and inhomogeneous broadening mechanisms is to be modeled.[52] It is known that the decay of the core excited state directly influences the energy resolution of the XES spectrum.[53] The lifetime of the core hole is given by $\tau_I = (D_I)^{-1}$ which leads, in a first approximation, to a Lorentzian line shape with the full-width at half-maximum height given by

$$\Delta\omega_I = D_I = (\tau_I)^{-1} = 2\Gamma_I \tag{8}$$

In principle, the analysis of the homogeneous broadening in the XES spectra would enable one to obtain the total decay rate of state $|I\rangle$ and compare it with the theoretical value of D_I (eq 5). However, the latter would require us to take account of the nonradiative dacay rates that are known to be dominated by the Auger process.[54] An in-depth study of this problem is beyond the scope of the present study.

The emission oscillator strength f_{IF} is related to the absorption oscillator f_{FI} strength as $f_{IF} = -f_{FI}$. The oscillator strength can be expanded as a power series in terms of the dimensionless fine structure constant α (= 1/137.03599). The first term in this expansion represents the electric dipole oscillator strength (f_{IF}^{ed}). For orientationally averaged transition rates, the term linear in α is zero, and the next leading term $\sim\alpha^2$ can be written as the sum of the electric quadrupole (f_{IF}^{eq}) and magnetic dipole (f_{IF}^{md}) oscillator strengths

$$f_{IF} = f_{IF}^{\mathrm{ed}} + f_{IF}^{\mathrm{md}} + f_{IF}^{\mathrm{eq}} \tag{9}$$

In atomic units, these three contributions to the oscillator strengths can be expressed as follows

$$f_{IF}^{\mathrm{ed}} = -\frac{2}{3} E_{IF} |\vec{m}_{IF}|^2 \tag{10}$$

$$f_{IF}^{\mathrm{md}} = -\frac{2}{3}\alpha^2 E_{IF} |\vec{\mu}_{IF}|^2 \tag{11}$$

$$f_{IF}^{\mathrm{eq}} = -\frac{1}{20}\alpha^2 E_{IF}^3 \sum_{a,b} |(Q_{ab})_{IF}|^2 \tag{12}$$

Here, E_{IF} is the transition energy between states $|I\rangle$ and $|F\rangle$, $\vec{m}_{IF}$, $\vec{\mu}_{IF}$, and $\{(Q_{ab})_{IF}\}$ are the corresponding matrix elements of the electric dipole, magnetic dipole, and electric quadrupole operators, respectively (see ref 49 for precise definitions).

In this work, the theoretical framework presented above has been implemented in a simple quasi-one-electron approach. In principle, the XES experiment involves the excitation of an electron from the 1s-orbital (of the XAS absorber being probed) into the continuum, thus forming a N-1 electron detached state. This state relaxes by emission of a photon from the higher lying 2sp, 3sp, or valence orbitals into the final N-1 electron state. Concomitant with the electron ejection, the valence and sub-valence orbitals experience an increased nuclear charge at the XAS absorber that will tend to distort the orbitals to some extent ("electronic relaxation"). This effect has previously been modeled by Glatzel and co-workers by running the calculations with an increased nuclear charge at the absorber atom.[18] However, they found that this approximate treatment of electronic relaxation did not improve the agreement between theory and experiment. Hence, we have resorted to the simplest possible approach in which the electronic relaxation in the intermediate state is neglected.

The orbitals used in the present treatment come from a density functional theory (DFT) calculation and satisfy the canonical Kohn−Sham equations

$$\hat{F}^{\sigma}|p_{\sigma}\rangle = \varepsilon_p^{\sigma}|p_{\sigma}\rangle \tag{13}$$

where $\hat{F}^{\sigma}$ is the Kohn−Sham operator; $|p_{\sigma}\rangle$ is a spin-orbital with spin $\sigma = \alpha,\beta$; and ε_p^{σ} is the orbital energy. The Kohn−Sham operator is

$$\hat{F}^{\sigma} = \hat{h} + \int \frac{\rho(\mathbf{r}')}{|\mathbf{r} - \mathbf{r}'|} d\mathbf{r}' + V_{\mathrm{XC}}[\rho](\mathbf{r}) \tag{14}$$

(51) Corney, A. *Atomic and Laser Spectroscopy*; Clarendon: Oxford, 1977.
(52) Petrenko, T.; Neese, F. *J. Chem. Phys.* **2007**, *127*, 164319.
(53) Krause, M. O.; Oliver, J. H. *J. Phys. Chem. Ref. Data* **1979**, *8*, 329.
(54) Schieffer, P.; Guivarc'h, A.; Lallaizon, C.; Lepine, B.; Sebilleau, D.; Turban, P.; Jezequel, G. *Appl. Phys. Lett.* **2006**, *89*, 161923.

where $\hat{h}$ is the one-electron Hamiltonian (kinetic energy plus electron-nuclear potential, together with other external potentials such as external electric fields which may be present). The second term presents the Coulomb repulsion, where

$$\begin{aligned}\rho(\mathbf{r}) &= \rho^{\alpha}(\mathbf{r}) + \rho^{\beta}(\mathbf{r}) \\ &= \sum_{i_\alpha} |i_\alpha(\mathbf{r})|^2 + \sum_{i_\beta} |i_\beta(\mathbf{r})|^2 \end{aligned} \quad (15)$$

is the electron density, and the exchange correlation potential is

$$V_{\mathrm{XC}}^{\sigma}[\rho](\mathbf{r}) = \frac{\delta E_{\mathrm{XC}}}{\delta \rho^{\sigma}(\mathbf{r})} \quad (16)$$

The quantity $E_{\mathrm{XC}}[\rho]$ is the exchange-correlation functional. Associated with the Kohn−Sham procedure is the ground state Kohn−Sham determinant

$$|G\rangle = |i...j...n| \quad (17)$$

In general, occupied orbitals of the electronic ground state are labeled with *i*,*j*,*k*, ... and unoccupied ones with *a*,*b*,*c*, ... In the one-electron approach, the initial core-excited and final states are constructed as

$$|I\rangle = |a...j...n| \quad (18)$$

$$|F\rangle = |a...i...n| \quad (19)$$

For the specific application at hand, orbital *i* is a core orbital, e.g., the metal 1s derived orbital of a given absorber atom; *a* is an arbitrary unoccupied orbital (or a continuum unbound one-electron level); and *j* is another semicore or valence orbital of the same atom.

Rather than trying to obtain accurate total energies for all of these states, the simple approximation is adopted for the emission energy

$$E_{IF}^{\sigma} = \hbar\omega_{IF}^{\sigma} = \varepsilon_j^{\sigma} - \varepsilon_i^{\sigma} \quad (20)$$

This is of course fairly simplistic. In terms of time-dependent DFT, it can be shown that the orbital energy difference is a well-defined approximation to the state energy difference if no Hartree−Fock exchange is present in the DFT potential.[55,56] For a semiquantitative discussion, this should be good enough since the substantial errors of the presently used DFT potentials prevent the calculations from predicting accurate absolute transition energies anyways (for reviews, see refs 57 and 58). In addition, we have consistently observed that core/valence excitations are strongly dominated by the orbital energy contribution since the contributions of the exchange-correlation kernel are very small for such excitations. In fact, for XAS calculations, the absolute transition energies obtained from the TD-DFT linear response equations and the orbital energy approximation differ by at most a few tenths of an electronvolt which is considered to be negligible for the present application.[59]

Equations 6−7 and 9−12 have been implemented into a development version of the ORCA electronic structure package.[39] The electric quadrupole and magnetic dipole contributions to the emission rate are calculated in a way previously discussed for X-ray absorption spectra.[49] As will be pointed out below, the electric dipole contributions have been found to be strongly dominant for XES calculations. Hence, while the final intensities do include the electric quadrupole and magnetic dipole contributions, we will not discuss their relative contributions below.

Obviously, the simple one-electron approximation falls short of properly including electronic relaxation, and hence one cannot model multielectron phenomena such as shake-up or shake-down transitions with such an approach. Second, the approach does not take proper care of multiplet effects since it is based on simple individual determinants that do not span the proper spin and space manifolds to provide the correct multiplet structure inherent in the multielectron nature of the electronic states that are involved. This is expected to adversely affect the results obtained for the Kβ main line but should be less serious for the valence to core region. Efforts are underway in our laboratories to remove the restrictions mentioned above.

Results. As anticipated from the discussion above, the Kβ main line region of the spectra is not particularly well-predicted by the simple one-electron-like DFT approach. First of all, the calculations underestimate the exchange-based splitting, thus pointing to deficiencies of the DFT potential in the semicore region (consistent with too small of a contribution from spin polarization[49,60]). Second, the calculations do not provide the correct intensity ratio of the two Kβ main line peaks presumably because multiplet effects are not properly treated. Hence, we will not examine this spectral region further in the present study but will instead concentrate on the valence to core region, which shows greater sensitivity to changes in the chemical environment. The valence to core XES spectra were calculated both at the experimental structures (method 1) and using geometry optimized structures (method 2), as described in the Experimental Section.

Figure 4 shows the relationship between the calculated valence to core energies and the experimental energies. The reported experimental energies correspond to the measured peak maximum in the valence to core region. Calculated energies were determined by applying a 2.5 eV broadening to the calculated valence to core spectra and reporting the energy of the highest intensity peak. Each dot in Figure 4 corresponds to one of the twelve complexes from this study, calculated using either method 1 (blue open circles) or method 2 (red dots). For both method 1 and method 2, the calculated absolute transition energies are underestimated. This is expected due to the limitations of DFT in modeling potentials near the nucleus and is analogous to the situation met in calculating XAS spectra. There we have shown that the underestimation depends on the particular DFT functional and the basis set used and is highly systematic. Hence, it can be dealt with by proper calibration, and the required energy shift at a given level of theory can be

(55) Petersilka, M.; Gross, E. K. U. *Int. J. Quantum Chem.* **1996**, *60*, 1393.
(56) Petersilka, M.; Gossmann, U. J.; Gross, E. K. U. *Phys. Rev. Lett.* **1996**, *76*, 1212.
(57) Neese, F. *Coord. Chem. Rev.* **2009**, *253*, 526.
(58) Neese, F. *J. Biol. Inorg. Chem.* **2006**, *11*, 702.
(59) Consider for example the system [Ni(LS,S)2] discussed previously: Ray, K.; DeBeer George, S.; Solomon, E. I.; Wieghardt, K.; Neese, F. *Chem.—Eur. J.* **2007**, *13*, 2753. DeBeer George, S.; Neese, F. *Inorg. Chem.* **2010**, *49*, 1849. Using the protocol discussed in: DeBeer George, S.; Neese, F. *Inorg. Chem.* **2010**, *49*, 1849. the TD-DFT transition energies for the lowest three excitations at the S-K-edge are 2409.248, 2410.337, and 2410.486 eV, respectively, and the corresponding eigenvectors consist to 99.9% of one single excitation. The simple one-electron approximation yields 2409.588, 2410.673, and 2410.816 eV. Thus, there is merely a small ∼ .3 eV shift to higher energy in the one-electron approximation, but overall little seems to be lost.
(60) Orio, M.; Pantazis, D. A.; Petrenko, T.; Neese, F. *Inorg. Chem.* **2009**, *48*, 7251.

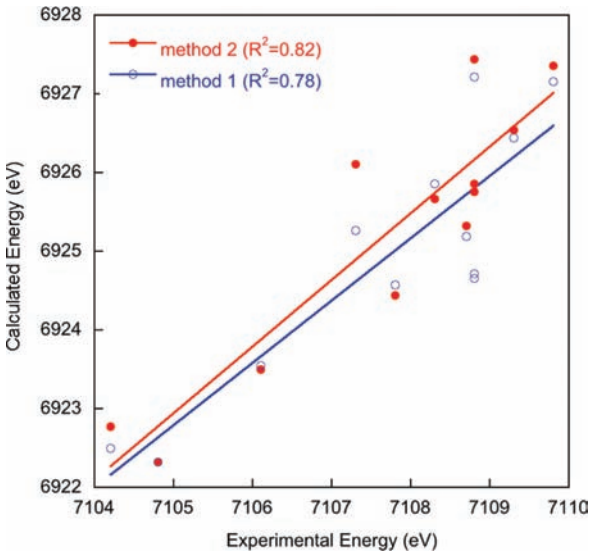

Figure 4. Experimental vs calculated valence to core energies using method 1 and method 2.

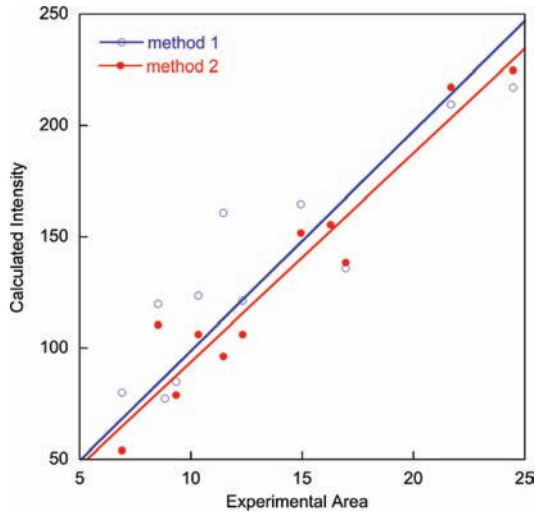

Figure 5. Experimental vs calculated valence to core intensities using method 1 and method 2. The lines have been forced through the origin and give slopes of 9.88 ± 1.87 (method 1) and 9.37 ± 1.39 (method 2).

determined.[48−50] For the presently employed method of calculation, the required shifts are of 182.7 ± 0.8 eV and 182.5 ± 0.8 eV for methods 1 and 2, respectively. This indicates that the geometry optimizations only affect the relative energy shift slightly and that the error in the predicted energy does not change. An extensive calibration study using different functionals and basis sets is outside the scope of this work but will be reported in due course.

Figure 5 presents the relationship between calculated total oscillator strength and the experimental areas (as reported in Table 2) for each of the 12 complexes examined in this study, using both method 1 (blue open circles) and method 2 (red dots). The total calculated oscillator strength is comprised of electric dipole, electric quadrupole, and magnetic dipole contributions. However, electric dipole contributions dominate (representing on average 97% of the calculated intensity). The relationship between experimental areas and total calculated intensity for the valence to core region, using method 1, is reasonably linear with a slope of 9.88 ± 1.87 (or an error of ∼19%). The errors in the calculated intensities are signficantly reduced upon using geometry optimized structures (method 2). Here, a slope of 9.37 ± 1.39 or an error of ∼14% has been found.

We note that the errors in both transition energies and intensities are larger than those observed for analogous TDDFT calculations of XAS spectra.[48−50] This may derive in part from the more simplified approach used for calculations of XES spectra and will be the subject of a more detailed investigation in future studies. However, it should also be noted that the experimental errors in transition energies and intensities are also larger for valence to core emission spectra than what we have previously reported for XAS spectra.[48−50] This orginates in part from the very weak signal relative to the background (resulting in larger uncertainties in experimental areas, ∼10% as discussed in the experimental), as well as from the method employed for energy calibration (which introduces an uncertainty of ±0.2 eV).

Having established acceptable linear correlations between experimental and calculated transition energies and intensities, it is instructive to examine the experimental data with respect to the calculated spectra. Figure 6 compares the experimental high-spin ferric spectra (A) to the calculated spectra (method 2) (B). A constant shift of 182.5 eV and a broadening of 2.5 eV have been applied to all calculated spectra. A parallel comparison for the ferrous complexes is made in Figure 7.

These comparisons demonstrate that in addition to predicting the relative energies and intensities the calculations also reliably predict the relative splittings and intensity distributions. It should be noted that in some cases features in the 7090−7100 eV "satellite region" are very weak or absent in the experimental spectra. However, this is at least in part due to the strong background from the Kβ main peak. In addition, there are experimentally observed features at ∼7115 eV that are not reproduced by the calculations. These transitions likely correspond to double photoionizations (i.e., Fe K + Fe L excitations), which could be eliminated by tuning the incident beam to lower energies. This will be the subject of future investigations. In any case, such multielectron excitations are not accounted for in our simple DFT approach. Nevertheless, the strong general agreement between experiment and theory allows us to use the calculations for a more detailed analysis of the information content of the valence to core spectra.

Nature of the Core/Valence Features. As noted above, the spectra are dominated by dipole allowed Fe np to Fe 1s transitions. Figure 8 presents the calculated spectrum of $[Fe(II)Cl_4]^{2-}$ together with representative molecular orbitals that dominate each set of observed transitions. The primary valence to core peak at ∼7109 eV arises from intermediate states with contributions from six molecular orbitals that are dominantly Cl 3p in character (two representative molecular orbitals are shown in Figure 8). A weak shoulder at ∼7111 eV corresponds to the transition from the t_2 set of 3d orbitals. The isolated peak at ∼7097 eV corresponds to transitions from dominantly Cl 3s-based molecular orbitals. In all cases, the transitions are dominated by a dipole mechanism. As will be elaborated below, the calculated intensity arises from 5−10% Fe np character mixed into each of the molecular orbitals.

Figure 9 shows the calculated spectrum of $[Fe(II)(tacn)_2]^{2+}$, together with the key molecular orbitals corresponding to the observed transitions. Similar to ferric tetrachloride, the valence to core spectrum is dominated by ligand p molecular orbitals, which have some (1−7%) Fe np character mixed in. A lower-energy feature appears at ∼7091 eV which corresponds to transitions from dominantly nitrogen, and to a lesser extent

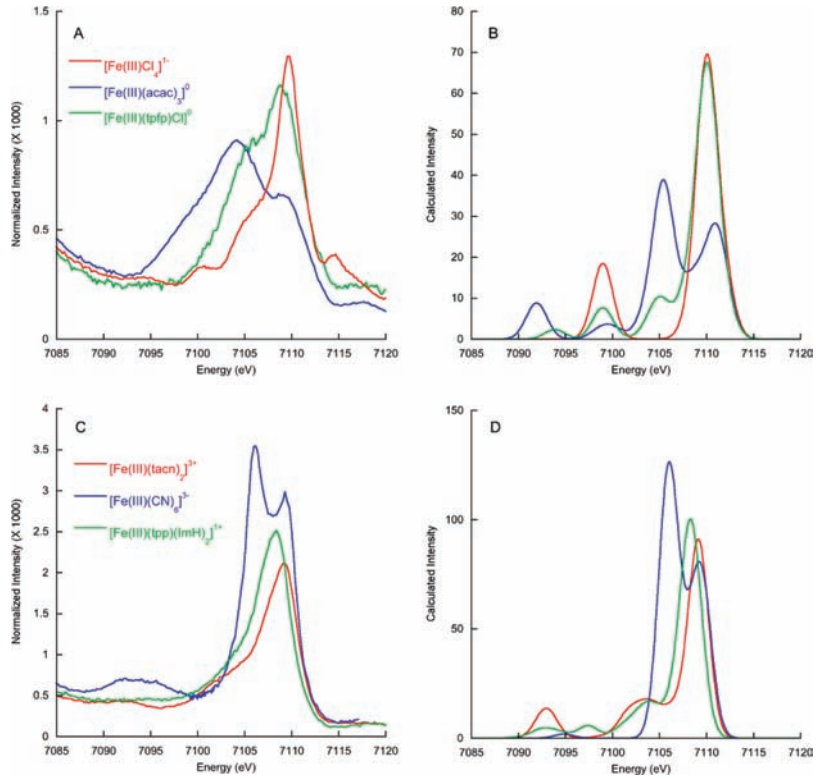

Figure 6. Experimental valence to core spectra for high-spin ferric complexes (A) and the corresponding calculated spectra (B). Experimental valence to core spectra for low-spin ferric complexes (C) and the corresponding calculated spectra (D). A 2.5 eV broadening and a constant shift of 182.5 eV have been applied to all calculated spectra.

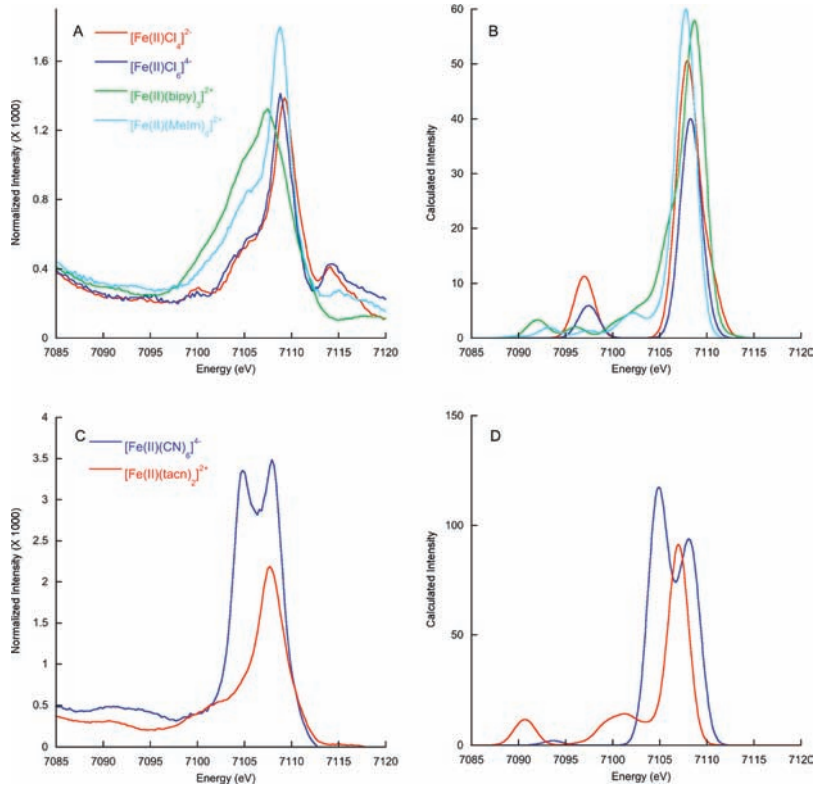

Figure 7. Experimental valence to core spectra for high-spin ferrous complexes (A) and the corresponding calculated spectra (B). Experimental valence to core spectra for low-spin ferrous complexes (C) and the corresponding calculated spectra (D). A 2.5 eV broadening and a constant shift of 182.5 eV have been applied to all calculated spectra.

carbon, 2s molecular orbitals. These features are shifted by ~6 eV relative to the satellite region in $[Fe(II)Cl_4]^{2-}$ and reflect a significant difference in the ligand Cl 3s and N 2s ionization energies. None of the intense transitions are associated with molecular orbitals having any significant d-character. The t_{2g} set of d-orbitals contributes as a very weak shoulder at ~7111

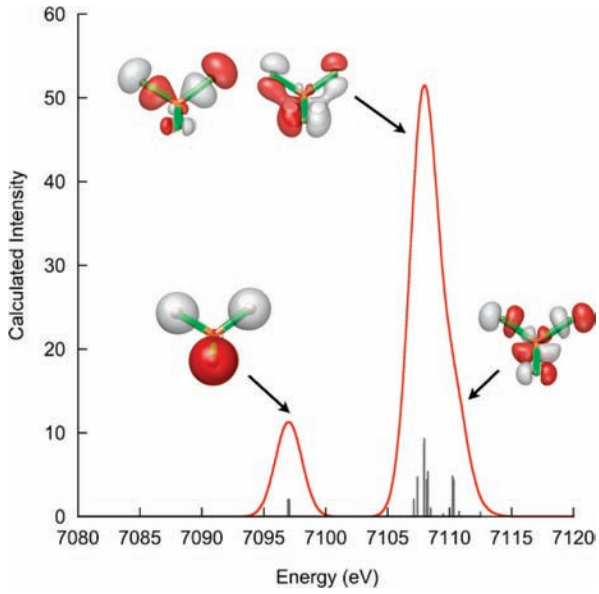

Figure 8. Calculated valence to core spectrum for $[Fe(II)Cl_4]^{2-}$ and key molecular orbitals contributing to the observed transitions.

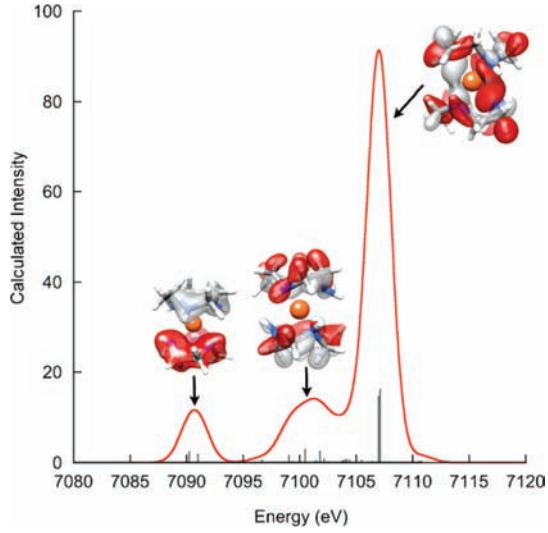

Figure 9. Calculated valence to core spectrum for $[Fe(II)(tacn)_2]^{2-}$ and key molecular orbitals contributing to the observed transitions.

eV, again demonstrating the dominantly dipole allowed nature of these transitions.

High-Spin vs Low-Spin Complexes. As noted above, the experimental valence to core data show an approximately 2-fold increase in intensity on going from high-spin to low-spin complexes. This difference is reproduced by the calculations; however, the origin of the intensity difference is not immediately obvious. To systematically understand the increased intensity on going to low-spin systems, we performed a series of in silico investigations on hypothetical molecules. Figure 10A shows the calculated spectra for high-spin T_d-$[Fe(III)Cl_4]^{1-}$, high-spin D_{4h}-$[Fe(III)Cl_4]^{1-}$, and hypothetical low-spin analogues. In all cases, the Fe−Cl bond was fixed at 2.15 Å. The distortion to D_{4h} perturbs the spectrum only slightly, increasing the transition energies by ∼0.2 eV and resulting in slightly increased intensities. It is clear, however, that there is very little geometric contribution to the observed intensities. Upon going to the hypothetical low-spin $[Fe(III)Cl_4]^{1-}$ complexes, the transition energies decrease by ∼1 eV relative to the high-spin complexes, indicating greater stabilization of the occupied ligand-based valence orbitals in the low-spin complexes due to increased bonding character. However, there is no significant change in intensity.

Having ruled out any significant direct contribution from geometry or spin state, we then examined the variation of the spectral features with respect to bond distances. A hypothetical series of D_{4h}-$[Fe(III)Cl_4]^{1-}$ complexes with Fe−Cl bonds ranging from 1.95 to 2.55 Å are shown in Figure 10B. The observed intensities clearly correlate with the Fe−Cl distances, decreasing essentially exponentially as the Fe−Cl bond is lengthened (Figure 11). Hence, these calculations indicate that the Fe np contributions to the valence orbitals are distance dependent and affect both the primary valence to core transition and the satellite transitions in a similar manner. The origin of the effect must be the increased ligand/Fe-np overlap that leads to stronger orbital interactions and hence more ligand/Fe-np orbital mixing.

However, the calculations do not indicate whether the contribution derives from the iron 3p or 4p orbitals. This is an important question in evaluating the possible contribution of 4p orbitals to bonding in transition metal complexes, which has been a subject of some controversy.[61−64]

To evaluate this question, an additional set of calculations were performed utilizing the ano-pVDZ basis set.[65] This is an atomic natural orbital basis set, which has the advantage that individual 3p or 4p orbitals can be cleanly identified in the basis set and hence also in the final molecular orbital vectors. Examination of the calculations for the hypothetical series of D_{4h}-$[Fe(III)Cl_4]^{1-}$ complexes (with Fe−Cl bonds ranging from 1.95 to 2.35 Å) showed that the calculated intensity is roughly proportional to the total p-character. However, there are significant contributions from both the Fe 3p and 4p orbitals to the calculated XES spectra. No significant Fe-2p or Fe-5p contributions were found. Therefore, one can attribute the observed effects on one hand to intensity borrowing from the Kβ main line (reflecting the Fe-3p contributions) and on the other hand to the Fe-4p contributions to bonding. Unfortunately, it appears to be difficult to cleanly separate these two important contributions to the observed intensity.

Correlation of Spectral Features with Ligand Identity. A final set of calculations addressed the key question of how the chemical identity of the ligands contributes to the valence to core region of the XES spectra. Figure 12 shows the calculated spectra for high-spin T_d-$[Fe(III)(X)_4]^{1-}$, where X is varied from PH_2^- to SH^- and Cl^- (top) and from NH_2^- and OH^- to F^- (bottom).

These two series allow us to evaluate the ligand 3s/3p (or 2s/2p in NH_2^-, OH^- to F^-) contributions to the spectra. On going from PH_2^- to SH^- to Cl^-, the ∼7110 eV feature increases in intensity and decreases in energy by ∼2 eV. A parallel, but more dramatic effect, is seen in the satellite region where the ∼7100 eV feature shifts by more than 3 eV over the series. This reflects the increase in the ligand 3s ionization energy on going from P to Cl. For the $NH_2^-/OH^-/F^-$ series, more pronounced changes are observed. The overall shape of the main

(61) Maseras, F.; Morokuma, K. *Chem. Phys. Lett.* **1992**, *195*, 500.
(62) Bayse, C. A.; Hall, M. B. *J. Am. Chem. Soc.* **1999**, *121*, 1348.
(63) Landis, C. R.; Cleveland, T.; Firman, T. K. *J. Am. Chem. Soc.* **1998**, *120*, 2641.
(64) Landis, C. R.; Firman, T. K.; Root, D. M.; Cleveland, T. *J. Am. Chem. Soc.* **1998**, *120*, 1842.
(65) Valeev, E.; Neese, F., unpublished results.

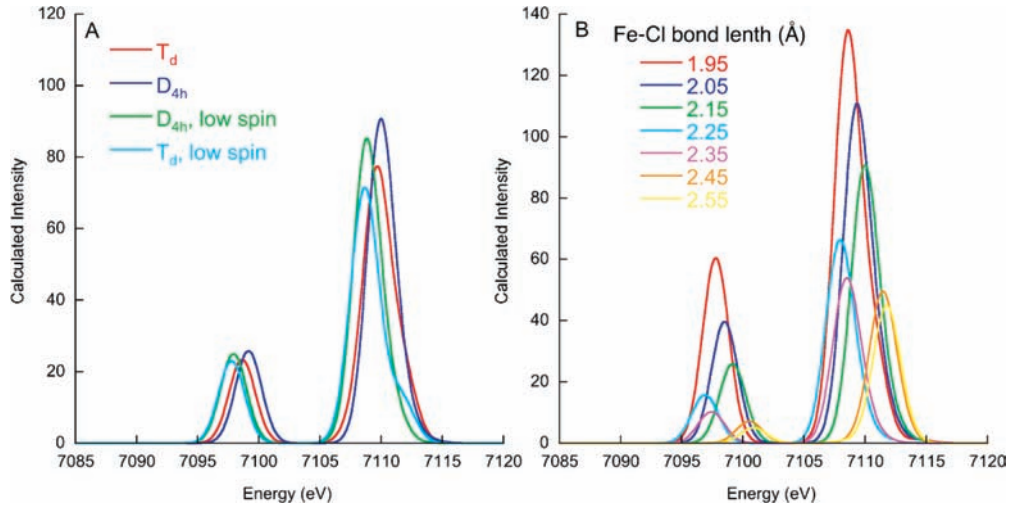

Figure 10. Calculated valence to core spectra for high-spin T_d-$[Fe(III)Cl_4]^{1-}$, high-spin D_{4h}-$[Fe(III)Cl_4]^{1-}$, and hypothetical low-spin T_d-$[Fe(III)Cl_4]^{1}$ and D_{4h}-$[Fe(III)Cl_4]^{1-}$ (A). Calculated valence to core spectra for high-spin D_{4h}-$[Fe(III)Cl_4]^{1-}$ at different Fe−Cl bond lengths (B).

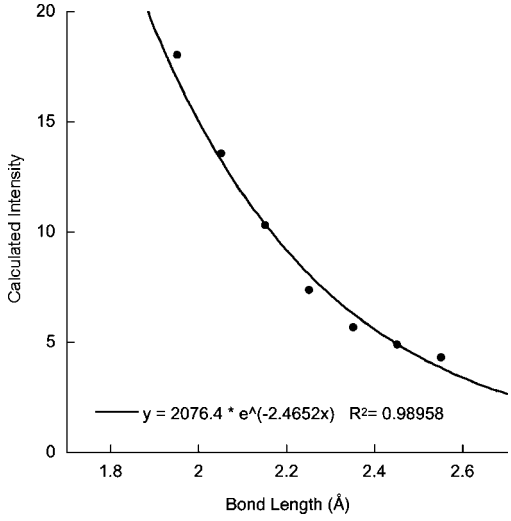

Figure 11. Relationship between bond length and the calculated intensity of the valence to core region.

∼7110 eV feature changes, and the satellite features shift by ∼6 eV in energy, reflecting a larger change in ligand 2s ionization energies than in the 3s ionization energies. The overall spectral intensity increases from NH_2^- to F^- consistent with the decrease in Fe−L bond length (from 1.96 Å for $[Fe(III)(NH_2)_4]^{1-}$; 1.90 Å for $[Fe(III)(OH)_4]^{1-}$; 1.83 Å for $[Fe(III)(F)_4]^{1-}$).[22]

It is also expected that the ligand hybridization and protonation state should contribute to the observed spectra. To investigate these possibilities, two additional sets of calculations were performed. Figure 13A shows a comparison of $[Fe(II)(NH_3)_6]^{2+}$ (sp^3 hybridized nitrogen) to $[Fe(II)(MeIm)_6]^{2+}$ (sp^2 hybridized nitrogen). These calculations demonstrate that on going from an sp^3 to an sp^2 ligand there is a clear effect on the satellite region of the spectrum, with the pronounced N 2s feature at ∼7093 eV decreasing in intensity and new features appearing at higher energy. The higher-energy features (∼7097−7102 eV) correspond to both N and C 2s contributions from the imidazole and clearly indicate that they are not "atomic" in origin but will vary in energy and intensity due to delocalization of s/p character over the ligand, indicating a molecular orbital description is most appropriate.

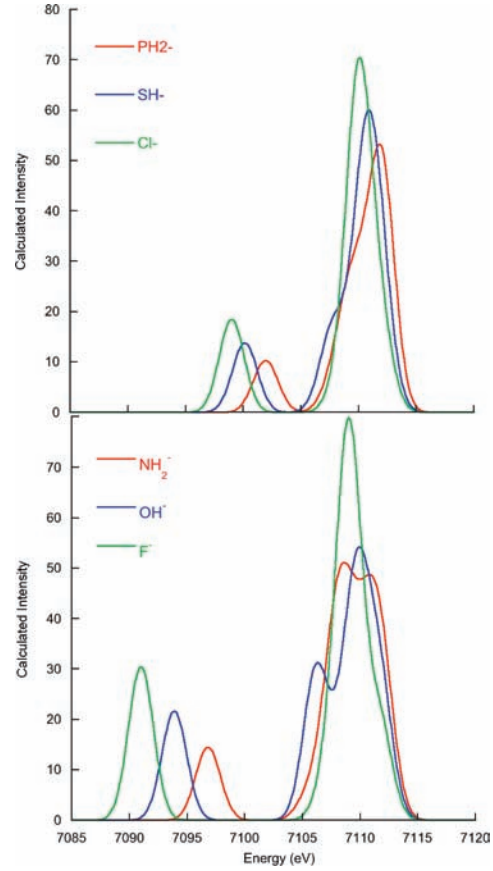

Figure 12. Calculated valence to core XES spectra for $[Fe(III)(X)_4]^{1-}$, where X is varied from PH_2^- to SH^- and Cl^- (top) and from NH_2^- and OH^- to F^- (bottom).

Figure 13B presents the valence to core XES calculations for $[Fe(IV)(O)(H_2O)_5]^{2+}$ and $[Fe(IV)(OH)(H_2O)_5]^{3+}$ in both $S = 1$ and $S = 2$ spin states. The calculated energies for the $S = 2$ complexes are ∼1 eV higher than the corresponding $S = 1$ complexes. For both Fe(IV)-oxo complexes, the $K\beta_{2,5}$ feature has decreased in intensity relative to the corresponding hyrdroxo complexes. Two features are apparent in the satellite region—a more intense feature at ∼7096 eV (dominated by O 2s contributions from the oxo group) and a weaker shoulder at

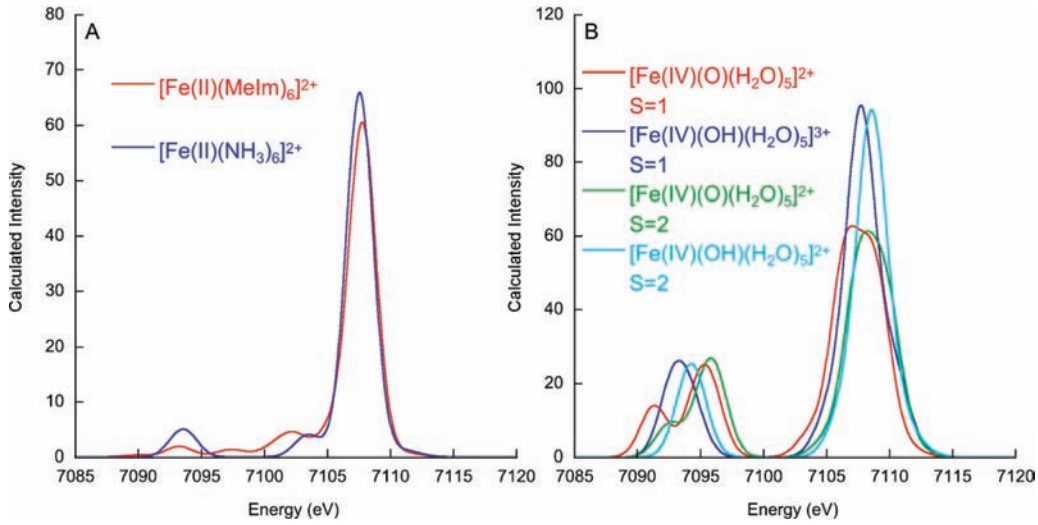

Figure 13. Calculated valence to core spectra for high-spin O_h $[Fe(II)(NH_3)_6]^{2+}$ to $[Fe(II)(MeIm)_6]^{2+}$ (A). Calculated valence to core spectra for $S = 1$ and $S = 2$ $[Fe(IV)(O)(H_2O)_5]^{2+}$ and $[Fe(IV)(OH)(H_2O)_5]^{3+}$ complexes (B).

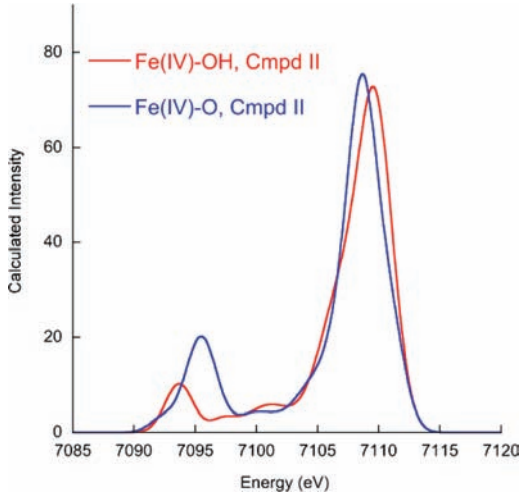

Figure 14. Calculated valence to core spectra for Fe(IV)−O and Fe(IV)−OH Compound II derivatives.

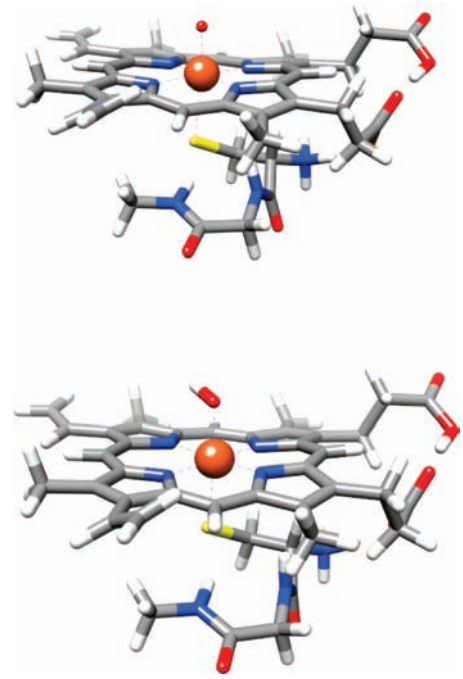

Figure 15. Active site models for Fe(IV)−O (top) and Fe(IV)−OH (bottom) Compound II derivatives. The structures (100 and 101 atoms, respectively) were optimized with the PBE functional and the SV(P) basis set.

∼7092 eV (corresponding to O 2s contributions of the coordinated waters). This ∼4 eV shift reflects the greater ease of ionization of O^{2-} as compared to H_2O and is consistent with trends observed in photoemission studies.[66] Upon going to the hydroxo complexes, a single feature at ∼7093 eV for the $S = 1$ complex (and 7094 eV for the $S = 2$ complex) is observed. This dominantly reflects contributions from the coordinated hydroxo group with weaker contributions from the waters. For the hydroxo complexes, the contributions from the water and the hydroxo are no longer resolved. This may be attributed to the shorter average Fe−OH_2 distance (1.92 Å) in the hydroxo complex as compared to the oxo complex (Fe−H_2O(avg) 1.98 Å). In either case, however, a ∼1.6 eV decrease in the energy of satellite feature is observed upon protonation. This indicates that Kβ XES in conjunction with molecular orbital calculations may be used as a sensitive probe of subtle perturbations at an iron site.

Applications to Compound II. One application where these methods may find utility is in the characterization of the compound II intermediates of heme enzymes. While for most heme enzymes the compound II intermediates are thought to be Fe(IV)-oxo species, Green and co-workers have shown that the compound II derivative of chloroperoxidase is a Fe(IV)−OH species.[14] More recent reports have indicated a mixture of Fe(IV)-oxo and Fe(IV)−OH species.[67] Due to the sensitivity of the Kβ region to the protonation state of an iron bound ligand, these methods may serve as an ideal way to distinguish these possibilities. Figure 14 shows the calculated valence to core XES spectra for thiolate-ligated Fe(IV)-oxo and Fe(IV)−OH heme complexes (as shown in Figure 15). Upon protonation, an ∼2 eV decrease in energy and a factor of ∼3 decrease in

(66) Ranke, W.; Kuhr, H. J. *Phys. Rev. B* **1989**, *39*, 1595.

(67) Stone, K. L.; Hoffart, L. M.; Behan, R. K.; Krebs, C.; Green, M. T. *J. Am. Chem. Soc.* **2006**, *128*, 6147.

intensity of the valence to core satellite is predicted, indicating that these two possibilities should be readily distinguished. However, these predictions await experimental verification.

Conclusions

A systematic experimental as well as computational study of the Kβ XES spectra for a series of ferrous and ferric complexes has been presented. The Kβ main line spectra are dominated by spin state contributions, while the valence to core spectra are affected by spin state, oxidation state, and coordination environment. Due to the greater spectral sensitivity of the valence to core region to changes in chemical environment, we have focused our efforts on understanding this region of the spectra. A straightforward DFT approach has been implemented. The generally good to excellent agreement between experiment and theory has allowed for a more detailed in silico investigation of the contributions to the experimental valence to core spectra. The spectra are dominated by dipole allowed Fe np to 1s transitions and are relatively insensitive to changes in the Fe site symmetry. However, changes in the spin state are shown to have pronounced contributions to both the intensity and energy distribution of the valence to core spectra. The decreased intensity of the high-spin complexes primarily derives from the longer iron−ligand bond lengths, which reduces iron np mixing with the ligand valence orbitals. The spectra are also shown to have a strong sensitivity to the ligand identity, showing ligand np and ns contributions, which are dependent on the identity (O, N, F), hybridization (sp^2 vs sp^3), and ionization state (O^{2-}, OH^-, H_2O) of the ligand.

These results indicate that the valence to core region of the XES spectra may have great utility for the examination of iron active sites in biological systems. The potential for application to heme protein intermediates has been discussed and computationally assessed. Key questions as to the identity of the central atom in nitrogenase and the nature of the O_2 binding mode in methane monooxygenase could be addressed and are the subject of ongoing studies in our laboratories. These applications clearly extend beyond iron active sites, where parallel developments for other transition metal active sites could answer key questions in biological and chemical catalysis.

Acknowledgment. We thank Prof. F. Ann Walker (University of Arizona) for kindly providing the [Fe(III)(tpp)$(ImH)_2$]Cl_2 sample for XES measurements. S.D. thanks the Department of Chemistry and Chemical Biology at Cornell University for generous financial support. F.N. gratefully acknowledges financial support from the University of Bonn, the Max-Planck society (via a "Max-Planck fellowship" to F.N.), and the SFB 813 'Chemistry at spin centers'. Portions of this research were carried out at the Stanford Synchrotron Radiation Lightsource, a national user facility operated by Stanford University on behalf of the U.S. Department of Energy, Office of Basic Energy Sciences. The SSRL Structural Molecular Biology Program is supported by the Department of Energy, Office of Biological and Environmental Research, and by the National Institutes of Health, National Center for Research Resources, Biomedical Technology Program.

Supporting Information Available: Representative fits to the valence to core spectra. This material is available free of charge via the Internet at http://pubs.acs.org.

JA101281E